62 71923   634

NASA TM X-99

GROUP 4
Downgraded at 3 year
intervals; declassified
after 12 years

TECHNICAL MEMORANDUM

X-99

PERFORMANCE OF A STRAIGHT STATOR AND A TILTED

STATOR TESTED WITH A HIGH-SOLIDITY HIGH-

PRESSURE-RATIO TRANSONIC ROTOR

By Ralph L. Schacht, Richard R. Cullom, and Arthur W. Goldstein

Lewis Research Center
Cleveland, Ohio

N 65   12689

(ACCESSION NUMBER)

(PAGES)

(NASA CR OR TMX OR AD NUMBER)

(THRU)

(CODE)

01

(CATEGORY)

DECLASSIFIED - EFFECTIVE 1-15-64
Authority: Memo Geo. Drobka NASA HQ.
Code ATSS-A Dtd. 3-12-64 Subj: Change
in Security Classification Marking.

NATIONAL AERONAUTICS AND SPACE ADMINISTRATION

WASHINGTON   October 1959

NATIONAL AERONAUTICS AND SPACE ADMINISTRATION

TECHNICAL MEMORANDUM X-99

PERFORMANCE OF A STRAIGHT STATOR AND A TILTED STATOR TESTED WITH

A HIGH-SOLIDITY HIGH-PRESSURE-RATIO TRANSONIC ROTOR*

By Ralph L. Schacht, Richard R. Cullom, and Arthur W. Goldstein

SUMMARY

An investigation was conducted to determine the overall stage and stator blade-element performance with a straight stator and a tilted stator in a transonic axial-flow-compressor stage. The performance data were compared to observe the effect of stator blade tilt on the weight-flow range. Both sets of stator blades were designed to operate near the rotor stall point and to attain the same performance level.

The tilted stator did not achieve the greater weight-flow range theoretically predicted. The acute corner made by the suction surface and the casing caused such high losses that they more than offset any gains predicted for tilted blades.

The straight-stator stage developed a pressure ratio of 1.24 at a maximum efficiency of 0.92 and an equivalent weight flow of 28.5 pounds per second in Freon 12 (equivalent value for air is 16.1 lb/sec) at the stator design speed of 288 feet per second in Freon 12 (622 ft/sec in air). For the tilted-stator stage, the pressure ratio, efficiency, and weight flow were 1.22, 0.85, and 31.6, respectively.

With supersonic stator inlet Mach numbers the stators stalled when the flow was tangent to the suction surface at the leading edge.

INTRODUCTION

To obtain compressors with high stage pressure ratios and large mass flow, considerable effort has been devoted to the development of compressors having supersonic velocities relative to the rotor. The major difficulty in the development of supersonic compressors is the

---

*Title, Unclassified.

large losses encountered in the stator (refs. 1 to 3). These losses re-
duce the adiabatic efficiency of the rotor-stator combination and there-
fore make the stage performance unattractive for practical application.
However, transonic compressors have operated successfully with good
stage pressure ratios and large mass flows, but again the stator seems
to limit the efficiency of the combination as the stator inlet Mach num-
bers are increased (ref. 4). Therefore, more knowledge of stator per-
formance in the transonic Mach number range is needed.

Another problem encountered is that of rotating stall at low rota-
tive speeds. This rotating stall results from insufficient flow range
of the inlet stages; it produces blade vibrational failures and contrib-
utes to poor engine acceleration. Thus, inlet stages with a large flow
range between choke and stall are desired.

The purpose of this investigation, carried out at the NASA Lewis
Research Center, was to investigate the range of performance of a set
of straight stator blades (i.e., sections designed along streamlines and
stacked on a radial line) and a set of tilted stator blades (i.e., ro-
tated about a streamline on the suction surface). Both sets of stator
blades were designed for the same rotor operating point. As discussed
in reference 5, the tilt of the stator blades reduces the effective an-
gle of attack for a given variation in flow angle, and thus the tests
should show the tilted-stator set to have increased range. Both sets of
blades were designed along the lines suggested by reference 6 specifi-
cally to cover the range of the high-solidity mixed-flow transonic rotor
tested in reference 7. The detailed blade-element data were taken at
both subsonic and transonic speeds in order to cover the stage range prob-
lem, which is generally a low-speed problem, and also the transonic-stator
problem, where additional data are required to determine the variation of
losses and of design incidence angle with increasing inlet Mach numbers,
particularly for double-circular-arc airfoil sections. In addition, very
little information has been presented to date concerning the variation
of low-loss incidence angle with stator inlet Mach number.

The overall performance of the transonic stage and the stator blade-
element data are presented for six corrected rotor tip speeds from 240 to
549 feet per second in Freon 12 (518 to 1184 ft/sec equivalent air values)
for both sets of stator blades. These rotor speeds produce stator inlet
Mach numbers from 0.5 to 1.1.

DESIGN

Rotor Design

The rotor used in this investigation was originally designed for
supersonic relative inlet Mach numbers (1.5 to 2.0). The original test

results are reported in reference 8. The rotor was then modified for transonic-type operation and reported in reference 7. The results of this test showed the rotor to have a large radial variation in work input; therefore, it was again modified for the present stator tests by contracting the passage height. The tip of the rotor blade was cut down from a 7-inch to a 6.72-inch radius at the exit. This increased the axial component and lowered the absolute discharge flow angles.

Stator Design

Both sets of stators were designed using stage flow range as the design criterion, as suggested by reference 6. According to this reference, two factors enter into the determination of flow range: (1) the surface-velocity-diffusion ratio

$$\left(\frac{\overline{v}}{V_3}\right)_S = \left(\frac{V_2}{V_3}\right)_S \frac{\sin \beta_{2,S}}{\sin \beta_{2,c}} \tag{1}$$

and (2) the range of incidence angle i. (Symbols are defined in appendix A.) The lower limit of angle of incidence may be either negative stall (angle less than the angle tangent to the pressure surface $\kappa_{p,2}$) or choke. The upper limit of angle of incidence may be either positive leading-edge stall (angle greater than the angle tangent to the suction surface $\kappa_{s,2}$) or excessive surface-velocity diffusion (separation on some downstream part of the blade). At low inflow Mach numbers, the incidence angle will be the limit. At high inflow Mach numbers, choke and surface-velocity-diffusion stall will limit the range. Figure 1 (redrawn from ref. 6) shows these general limits.

The rotor was considered to be a flow generator to be used for a study of stator range. No effort was made to design an acceptable stage. The design for both sets of stators was picked at a rotor tip speed of 288 feet per second in Freon 12 (622 ft/sec in air).

Both sets of stators were designed to operate near the rotor stall point. This point was selected in order to utilize as much of the rotor range as possible. Thus, both sets of stators were designed for a point (rotor stall) that is normally considered to be an off-design point of operation. The negative-stall angle of the straight stator was selected to be close to the experimentally determined flow discharge angle at rotor choke. The straight blade could thus be tested over its entire range, whereas the tilted blade might be limited by the rotor range because of the reduction in the effective angle of attack caused by the tilting. The tilted blades were tilted 45° about the stall flow angle, because the analysis showed this angle was large enough to show a substantial range effect. No exact value for a limiting surface-diffusion
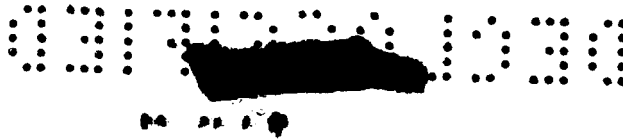
parameter has been established. For this design, a value of $(\overline{v}/V_3)_S =$ 1.62 was used, because separation was not expected with this value.

The velocity ratio at stall and the stall angle determined the flow condition at the mean radius. With the assumption of radial equilibrium of the flow, calculations of conditions at the rotor hub exit showed that the leading-edge wedge angle $(\kappa_{s,2} - \kappa_{p,2})$ of the stator hub would be very small if designed for the rotor exit conditions. The hub leading-edge wedge was therefore increased, which resulted in a blade design that would reach the assumed diffusion limit at the hub as the flow was reduced; leading-edge stall would occur at some lower flow.

To preserve the assumed velocity and flow angles at the mean section, the leading-edge wedge angle at the stator tip was decreased in view of the increase at the hub. Consequently, stall at the tip leading edge would occur at a higher flow than that at which the assumed diffusion limit would be reached, while the blade at the mean section would approach leading-edge stall and the assumed diffusion limit at the same flow.

A photograph of the rotor and straight stator is shown in figure 2. Figure 3 shows the rotor and tilted stator. Table I gives the blade geometry of both stators, and table II gives the blade coordinates. Note that neither stator blade was designed to turn the flow back to the axial direction. Since no special problems would be encountered in the design of another set of blades to accomplish this turning, the blades were not constructed.

APPARATUS

The stators were tested with Freon 12 as the working fluid in a closed system, as shown in figure 4. The rotor was driven by a 1500-horsepower variable-frequency motor through a gear train. The pressure developed by the stage was dissipated across the discharge throttle at the end of the radial diffuser (fig. 5). The gas flowed from the discharge collector through twin cooler assemblies to the inlet tank. An additional throttle was used in the inlet to control the pressure on the coolers.

INSTRUMENTATION AND PROCEDURE

Inlet stagnation temperatures and pressures were measured in the surge tank. Four static-pressure taps in the inlet nozzle were used for determining the weight flow, using the nozzle calibration from numerous previous surveys at station 1. The test section and the measuring

E-236

stations are shown in figure 5. The variations of the rotor discharge flow were determined at station 2 (about 0.64 in. downstream of rotor hub and 1.69 in. upstream of straight stator) by 8-point radial surveys using three combination probes at three circumferential positions. The total pressure, total temperature, static pressure, and angle were obtained from these probes (fig. 6).

Measurements of the stator discharge flow were made at station 3, about 0.50 inch downstream of the straight stator. The same axial positions were used for location and test measurements of the tilted and the straight stators. Eight-point radial surveys were made using four combination probes and two 13-tube total-pressure rakes. The 13-tube circumferential rakes were set at the average flow angle obtained from the four combination probes. The rakes were then reset at the average flow angle minus 3° and data were retaken. Data were again taken with the rakes reset at the average flow angle plus 3°. This procedure was followed to give the effective coverage of a 39-tube rake, so that circumferential variation of total pressure behind the stators could be obtained very accurately.

Static taps were installed in the casing over the rotor and stator and on the anterior portion of the stator suction surface at the hub, mean, and tip sections. These taps were used for positioning the shock at the stator throat.

The most reasonable evaluation of the reliability of the pressure measurements is believed to be the comparison of the weight flows computed from surveys at stations 2 and 3 and the nozzle calibration. The surveys at the higher speeds checked within ±4 percent of the nozzle weight flows. At the lower speeds a somewhat greater variation was obtained. It must be remembered that the rotor and stator absolute discharge angles were in the 30° to 60° range where a 2^O error in angle measurement can cause errors of ±4 percent of the nozzle weight flows.

The performance of the stage was determined over a range of back pressures from open throttle to nearly closed throttle for six speeds from corrected rotor tip speeds of 240 to 549 feet per second in Freon 12. The inlet-tank pressure was maintained at atmospheric pressure. The inlet-tank total temperature varied from 65° to 135° F, depending on the load on the cooling system. Freon purity was maintained above 97 percent at all times.

The spike-type thermocouples used on the combination probes at stations 2 and 3 were calibrated in air. Since the tests were conducted in Freon 12, a correction was applied that corrected the calibration from air to Freon 12. This correction is derived in appendix B.

RESULTS AND DISCUSSION

Overall Performance

The stators operated at both subsonic and supersonic inlet Mach numbers. At low rotor tip speeds (240, 288, and 336 ft/sec in Freon 12), the flow into and through the stators was subsonic. When a tip speed of 432 feet per second (Freon 12) was attained, the stator throat allowed the internal shock system of the rotor to pass on through the stators to some point in the passage downstream of the stators, resulting in supersonic flow into and through the stators. At this or higher tip speeds, closing the throttle forced a shock up into the stators. The shock could be positioned at the throat of the stators by increasing the back pressure. This gave the most efficient stage operation for these higher speeds where supersonic operation was possible. Closing the throttle more caused a slight reduction in weight flow and forced the shock system into the rotor, again giving subsonic flow into and through the stators. The shock could not be stabilized in the section between the rotor and stator.

The performance of the rotor and the straight-stator stage as measured at station 2 (about 0.64 in. downstream of the rotor hub) and station 3 (about 0.50 in. downstream of the stator tip) is shown in figure 7 as plots of total-pressure ratio and adiabatic efficiency against equivalent weight flow. The same parameters are plotted in figure 8 for the tilted-stator stage. At the stator design speed (288 ft/sec in Freon 12), the maximum efficiency (0.92) for the straight-stator stage was attained at a pressure ratio of 1.24 and a corrected weight flow of 28.5 pounds per second of Freon 12 (equivalent value for air is 16.1 lb/sec). For the tilted stator, the maximum efficiency and the pressure ratio and weight flow at this point were 0.85, 1.22, and 31.6, respectively. At the highest rotor speed tested (549 ft/sec in Freon 12), the peak efficiency was 0.78 at a pressure ratio of 2.03 and a corrected weight flow of 51.2 pounds per second of Freon 12 for the straight-stator stage. The equivalent values for the tilted stator were 0.73, 1.90, and 51.8. (The key in fig. 7 gives the equivalent rotor tip speeds for air and Freon 12. Hereinafter all rotor tip speeds will be given for Freon 12.)

The performance of the rotor as measured with the straight stator was not exactly the same as with the tilted stator. Any radial distribution of the flow caused by the stators affects the rotor performance; and, since the modified rotor was not tested by itself, no data were available for checking the effects of the stators on the rotor performance.

The solid symbols in figure 7 are the stall and wide-open-throttle operating points of the transonic rotor alone before modification, as reported in reference 7. The straight stators at the low operating speeds

E-236

did not decrease the operating range of the rotor. The three highest speeds for the highest corrected weight flows showed that the total-pressure ratio across the stator P_3/P_2 varied while the total-pressure ratio across the rotor P_2/P_1 and the weight flow remained essentially fixed. This shows that the stator choked first. If the rotor had choked first, P_2/P_1 and P_3/P_2 would both vary while the flow remained fixed.

The plots in figures 7 and 8 show that the straight stator achieved a higher pressure ratio and a higher efficiency than the tilted stator. The effective flow range of both stators was roughly the same, although both the stall and choke flows of the tilted-stator stage were increased about 2 pounds on the corrected-weight-flow scale.

Stator Inlet Flow

The radial variations in stator absolute entrance flow angle β_2 as measured from the axial direction and in absolute entrance Mach number M_2 for both sets of stators are shown in figure 9. These variations are shown for two of the six rotor speeds tested for two different operating conditions. The stall points are shown in figure 9(a), and the maximum-weight-flow points in figure 9(b). The two rotor tip speeds of 549 and 288 feet per second effectively show the range of inlet Mach number and flow angle covered by the tests.

The radial variation of stator inlet absolute Mach number was small at all speeds tested. At speeds where the stator inlet Mach number was subsonic, the absolute inlet Mach number was slowly reduced as the flow was reduced while operating at constant speed. At higher speeds with supersonic-type operation, the stator inlet Mach numbers and flow could not change until the shock system was pushed forward of the stator throat section.

The Mach numbers were effectively the same for both sets of stators. This was expected, since both sets of stators were designed for the same operating point.

The radial distribution of stator absolute entrance angle was approximately the same for comparable operating points at rotor speeds of 240, 288, and 336 feet per second. At higher speeds, the radial variation of stator entrance angle increased for operation at the maximum-flow points. The radial variation of the stator absolute entrance angle at the stall points was approximately the same for all speeds tested. Figure 9 also shows the pressure- and suction-surface stator blade angles $\kappa_{p,2}$ and $\kappa_{s,2}$. The stall-point absolute flow angles approximately follow the

shape of the stator suction-surface blade-angle distribution with radius at all speeds. The suction-surface blade angle sets the stall angle for stator operation with supersonic-type operation. The absolute flow angles for the tilted stator were higher at both ends of the operating flow range than those measured for the straight stators. Effectively, the overall flow range was still the same for both sets of blades.

Stator Exit Flow

The radial variations in stator absolute discharge angle β_3 and Mach number M_3 for the straight stators are shown in figure 10. These variations are shown for three different operating conditions for each of the six rotor speeds studied. The open-throttle points are given only to show that the flow expands through the stators to higher supersonic Mach numbers if no back pressure is imposed on the stators at the three highest speeds. For practical operation, a back pressure is imposed so that a shock system is forced up to the throat section of the stators. Considering only maximum-efficiency and stall points of operation, the radial variation of stator discharge Mach number is small at all speeds tested.

The trailing-edge blade angles of the suction and pressure surfaces $\kappa_{s,3}$ and $\kappa_{p,3}$ and the design flow angles are shown in figure 10. The flow angles leaving the straight blades at the design point (288 ft/sec tip speed and at stall) were approximately 3° higher than predicted (fig. 10(b)).

The exit absolute flow angles β_3 and Mach numbers M_3 for the tilted stators are compared with those for the straight stator in figure 11. The exit Mach numbers are slightly lower than those of the straight stators. The exit absolute flow angles show considerable unexplainable overturning at all radii.

Straight-Stator Blade-Element Characteristics

Since the gain in range was not achieved by the tilted stator, the detailed blade-element data will be presented only for the straight blade. A later section will compare the losses of the two stators and show to some extent what caused the trouble with the tilted stator.

The blade-element characteristics are presented in figure 12. The data are presented for the six rotor speeds tested for three of the eight radial stations from hub to tip. The radial stations presented, 5.46, 6.06, and 6.46 inches, represent the trends of the data in going from

near the hub to near the tip. The blade-element data are presented as plots of stator inlet Mach number M_2, total-pressure-loss coefficient $\bar{\omega}$, diffusion factor D, and axial-velocity ratio $V_{z,3}/V_{z,2}$ against stator suction-surface incidence angle i_s.

The stator total-pressure-loss coefficient is defined as the ratio of the difference between the inlet free-stream total pressure and the outlet averaged total pressure to the difference between the inlet total and static pressures.

The equation for the diffusion factor (ref. 9) is

$$D = \frac{V_2 \sin \beta_2 - V_3 \sin \beta_3}{2\sigma V_2} + 1 - \frac{V_3}{V_2} \tag{2}$$

The suction-surface incidence angle i_s is the angle between the tangent to the suction-surface leading edge and the inlet flow velocity vector.

For all radial sections, increasing the rotor speed or Mach number increased the magnitude of the minimum value of the total-pressure-loss coefficient. The incidence angle at which the minimum total-pressure-loss coefficient occurred also increased, and the low-loss incidence-angle range was reduced as the Mach number was increased.

The minimum total-pressure-loss coefficient approximately doubled as the speed was increased from 480 to 549 feet per second in Freon 12, even though at most radii the Mach number level increased only slightly. Mach numbers are above 1.0 at a tip speed of 549 feet per second at all radial sections. As pointed out in reference 4, any increase in stator inlet Mach number when the values are in the transonic range produces a stronger shock-wave system and associated higher losses. This rapid increase in total-pressure-loss coefficient is similar to the loss variation observed in many transonic rotors (ref. 10). In a rotor, however, the work input also increases as the Mach numbers are increased, so that the decrease in efficiency is not as large as that caused by increased losses due to increased Mach numbers in the stator.

The magnitude of the minimum total-pressure-loss coefficient increased quite rapidly at the tip. The stator diffusion factor does not explain this increase, since the diffusion factor was higher at the hub than at the tip. The increased losses at the tip must therefore be attributable to separation of the boundary layer at the tip, since the tip inlet wedge was decreased as explained in the design section and therefore separation of the boundary layer due to angle of attack should be expected.

At stall, the diffusion factor had a range of values from about 0.3 to 0.55 as the rotor speed was changed. This range of values was approximately the same for all radii.

The general limit lines comparable to figure 1 have been added to the curves of Mach number against suction-surface incidence angle in figure 12. On each curve the value of the surface diffusion $(\overline{v}/V_3)_S$ computed from equation (1) (derived in ref. 6) is listed for each of the stall points. Stall limit in this case is defined as the flow angle where the inlet flow becomes unstable. The value of $(\overline{v}/V_3)_S$ covers a range from 1.64 to 2.08. If all the surface-velocity-diffusion factors are averaged, a value of 1.84 is obtained. The overall performance data (fig. 7) show the stage stall line to be approximately the same as the stall line found in tests of the unmodified rotor alone. Since the modified rotor was never operated without stators, one can only say that the complete stage stalled but cannot positively assert that the stator itself caused stall. Another reason for not picking a definite $\overline{v}/V_3$ for stall is that one radial section could have caused stall. If all sections stalled at once, $(\overline{v}/V_3)_S = 1.84$ is a reasonable average value. If the tip caused the stall, the average value of $(\overline{v}/V_3)_S$ would be about 1.92. The mean radii show about a 15-percent increase in $(\overline{v}/V_3)_S$ as the tip speed is increased from 288 to 549 feet per second. The stator inlet Mach number at the stall point varies from 0.61 to 1.07 for the same change in tip speed. For design purposes, the value of $(\overline{v}/V_3)_S$ was assumed to be 1.62. At the stall point the measured value at the mean radius for the design speed of 288 feet per second was 1.64.

The data at low Mach numbers show that stall does not occur at the suction-surface blade angle $\kappa_{s,2}$ as predicted by reference 6, but occurs at an angle approximately 4° greater than $\kappa_{s,2}$. At the three highest speeds, where supersonic operation occurs, the suction surface does set the stall angle.

From table I, one sees that the straight-stator leading-edge wedge angles at the three radii are: 10.2^O at $r = 5.470$, 13° at $r = 6.000$, and 17.16^O at $r = 6.483$. Reference 6 predicts this wedge angle to be also the flow range of the blades at below design speed for these radii. The data show this magnitude for the flow range, but the choke and stall angles β_c and β_S are approximately 4° greater than predicted.

Tilted-Stator Blade-Element Characteristics

The blade-element characteristics of the tilted stator will not be given in great detail; however, some comparisons with the straight stator

will be made. Figure 13 shows plots of loss coefficient against radius for both the straight and tilted stators. The two operating points are representative of the data at all operating points. The total-pressure-loss coefficient is very high near the tip region. At the mean radii the losses are approximately the same as those measured for the straight stators, and at the hub the losses are lower than those measured for the straight stators.

The sketch in figure 14(a) shows that the designer has a choice whether the suction surface makes an acute angle with the hub or with the tip when blade tilt is prescribed for a blade. The tilted blades for this design were tilted so that an acute angle was obtained between the suction surface and the tip casing. The flow in this corner seems to have aggravated the already poor flow region normally found wherever the suction surface of a blade meets a wall. The suction surface of the blade at the hub made an obtuse corner with the hub, and exceptionally low losses were measured in this region. Further research is needed to see whether a combination of tilt at the hub plus a straight blade at the tip or some other configuration using tilt at both hub and tip and still obtaining obtuse corners with the suction surface (fig. 14(b)) would help solve the range and loss problem encountered in stators in the transonic Mach number region.

SUMMARY OF RESULTS

An axial-flow-compressor stage was tested with straight and with tilted stator blades in Freon 12 to investigate stator flow range and to obtain stator blade-element data for transonic stator inlet Mach numbers. The following results were obtained from this investigation:

1. The straight-stator stage developed a pressure ratio of 1.24 at a maximum efficiency of 0.92 and an equivalent weight flow of 28.5 pounds per second in Freon 12 (equivalent value for air is 16.1 lb/sec) at the stator design tip speed of 288 feet per second in Freon 12 (622 ft/sec in air). For the tilted stator the pressure ratio, efficiency, and weight flow were 1.22, 0.85, and 31.6, respectively.

2. At the highest rotor speed tested (549 ft/sec in Freon 12, 1184 ft/sec in air), the peak efficiency for the straight-stator stage was 0.78 at a pressure ratio of 2.03 and a corrected weight flow of 51.2 pounds per second of Freon 12.

3. The tilted-stator stage did not achieve a greater flow range than the straight-stator stage as theoretically predicted. The acute corner made by the suction surface and the casing caused such high losses that they apparently more than offset any gains obtained by tilting the blades.

4. With supersonic-type operation, the stators apparently stalled when the flow was tangent to the suction surface at the leading edge. At low speeds with subsonic-type operation of the stators, the stall angle was approximately 4° greater than the suction-surface blade angle.

5. The low-speed weight-flow range of operation was of the magnitude predicted by reference 6 (equal to the inlet blade wedge) but was displaced on the weight-flow scale.

6. The average stall surface-velocity-diffusion factor for the stators was approximately 1.84.

7. Increasing the inlet Mach number increased the magnitude of the minimum value of the total-pressure-loss coefficient and increased the inlet flow angle at which this minimum occurred.

8. With supersonic-type operation, placement of the shock system at the stator throat gave the most efficient stage operation.

Lewis Research Center
    National Aeronautics and Space Administration
   Cleveland, Ohio, August 4, 1959

APPENDIX A

SYMBOLS

c   chord, in.

D   diffusion factor

i   angle of incidence, angle between tangent to stator suction-surface leading edge and absolute velocity vector, deg

l length of straight section on suction surface at trailing edge, in.

M   absolute Mach number, ratio of absolute velocity of fluid to local velocity of sound

N   number of blades

P   absolute stagnation pressure, lb/sq in.

Pr   Prandtl number

R,X,Y,Z   blade coordinates (tables I and II)

R.F.   recovery factor

r   radial distance from axis of rotation, in.

$r_{\mathscr{C}}$ radius of curvature of suction-surface leading edge, in.

s   blade spacing, in.

T   local temperature of moving stream, ^{O}R

t   blade thickness, in.

V   absolute velocity, ft/sec

$\overline{V}$ average suction-surface velocity, ft/sec

β   fluid flow angle, angle between axis of rotation and absolute velocity vector, deg

γ   ratio of specific heats

γ^{o} blade-chord angle, angle between axis of rotation and blade chord, deg

Δ $1 - (T_i/T_a)$
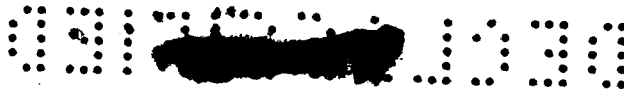
ϵ angle of tilt, deg

η adiabatic efficiency

κ blade angle, angle between tangent to blade surface and axial direction, deg

σ solidity, ratio of chord to spacing

$\bar{\omega}$ total-pressure-loss coefficient

Subscripts:

a   total or stagnation

c   choke operating condition

d   design

h   hub

i   indicated

l lower surface

p   pressure surface

S   stall operating condition

s   suction surface

t   tip

u   upper surface

z   axial direction

1   station 1, at rotor entrance

2   station 2, at rotor exit (stator entrance)

3   station 3, at stator exit

E-236

APPENDIX B

CORRECTION FOR SPIKE-TYPE-THERMOCOUPLE CALIBRATIONS

FROM AIR TO FREON 12

Reference 11 shows that, for high-velocity flow for a flat plate with turbulent boundary layer, the recovery factor is

$$R.F. = (Pr)^{1/3} \tag{B1}$$

where Pr is the Prandtl number, and the temperature recovery factor is defined as

$$R.F. = \frac{T_i - T}{T_a - T} \tag{B2}$$

where T_i is the adiabatic indicated wall temperature, T is the local temperature of the moving stream, and T_a is the total or stagnation temperature.

For an ideal gas,

$$\frac{T_a}{T} = 1 + \frac{\gamma - 1}{2} M^2 \tag{B3}$$

Substituting (B1) and (B3) in equation (B2) gives

$$\frac{T_i}{T} = 1 + \frac{\gamma - 1}{2} M^2 (Pr)^{1/3} \tag{B4}$$

The air calibration of the probes was expressed in terms of the parameter

$$\Delta = 1 - \frac{T_i}{T_a} \tag{B5}$$

Substituting (B4) and (B3) in (B5) gives

$$\Delta = \frac{\frac{\gamma - 1}{2} M^2 \left[1 - (Pr)^{1/3} \right]}{1 + \frac{\gamma - 1}{2} M^2} \tag{B6}$$

Figure 15 shows the original calibration for six probes in air. The dashed curve shows the theoretical flat-plate curve for air, using equation (B6). The fit is fairly good up to Mach 1.0. Above Mach 1.0

the thermocouple would always be behind a strong shock system caused by the rest of the instrument; therefore, the thermocouple would always see some kind of subsonic correction.

With this reasoning, the air calibration was corrected to a Freon 12 calibration by the following:

$$\Delta_{\text{Freon 12}} = \frac{\Delta_{\text{Freon flat plate}}}{\Delta_{\text{Air flat plate}}} \Delta_{\text{Air measured}}$$

Figure 15 also shows the calibration curve finally used for Freon 12.

One indication of the accuracy of the temperature measurements is given by comparing the efficiencies as calculated using moment-of-momentum calculations with those using the thermocouple data. This comparison showed the thermocouple efficiencies to be approximately 4 percent higher than the momentum efficiencies. This agreement is considered satisfactory, since the temperature rises for a single stage are very small, especially when tested in Freon 12 where the temperature rise amounts to approximately one-third of the rise in air. Therefore, any small error in temperature measurement or Mach number correction shows up as a larger error when calculating the efficiency. It should be noted that these apparent errors in temperature have little effect on the stator performance.

REFERENCES

1. Klapproth, John F., Ullman, Guy N., and Tysl, Edward R.: Performance of an Impulse-Type Supersonic Compressor with Stators. NACA RM E52B22, 1952.

2. Hartmann, Melvin J., and Tysl, Edward R.: Investigation of a Supersonic-Compressor Rotor with Turning to Axial Direction. II - Rotor Component-Off-Design and Stage Performance. NACA RM E53L24, 1954.

3. Wilcox, Ward W.: Investigation of Impulse-Type Supersonic Compressor with Hub-Tip Ratio of 0.6 and Turning to Axial Direction. II - Stage Performance with Three Different Sets of Stators. NACA RM E55F28, 1955.

4. Cullom, Richard R., Montgomery, John C., and Yasaki, Paul T.: Experimental Performance of a 0.35 Hub-Tip Radius Ratio Transonic Axial-Flow-Compressor Stage Designed for 40 Pounds per Second per Unit Frontal Area. NACA RM E58D04a, 1958.

5. Goldstein, Arthur W., and Schacht, Ralph L.: Performance of a Super-
   sonic Compressor with Swept and Tilted Diffuser Blades. NACA RM
   E54L29, 1955.

6. Goldstein, Arthur W., and Schacht, Ralph L.: Relation Between Flow
   Range and Other Compressor-Stage Characteristics. NACA RM E58B24,
   1958.

7. Neumann, Harvey E.: Performance of a High-Solidity High-Pressure-
   Ratio Transonic Rotor. NACA RM E55I19, 1955.

8. Schacht, Ralph L., Goldstein, Arthur W., and Neumann, Harvey E.:
   Performance of a Supersonic Rotor Having High Mass Flow. NACA RM
   E54D22, 1954.

9. Lieblein, Seymour, Schwenk, Francis C., and Broderick, Robert L.:
   Diffusion Factor for Estimating Losses and Limiting Blade Loadings
   in Axial-Flow-Compressor Blade Elements. NACA RM E53D01, 1953.

10. Schwenk, Francis C., Lewis, George W., and Hartmann, Melvin J.: A
    Preliminary Analysis of the Magnitude of Shock Losses in Transonic
    Compressors. NACA RM E57A30, 1957.

11. McAdams, William H.: Heat Transmission. McGraw-Hill Book Co., Inc.,
    Third ed., 1954, pp. 309-312.

E-236

CF-3

E-236
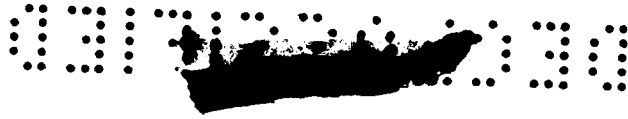
TABLE I. - STATOR BLADE GEOMETRY
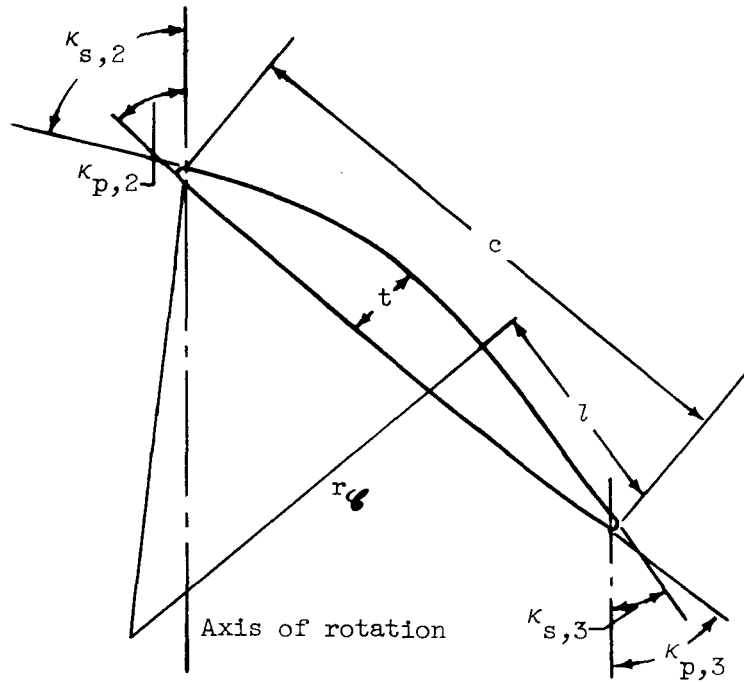
	Straight stator			Tilted stator		
r, in.	5.470	6.000	6.483	5.470	6.000	6.483
$\kappa_{s,2}$, deg	44.9	48.0	52.9	55.33	57.52	60.98
$\kappa_{p,2}$, deg	34.7	35.0	35.74	45.33	40.43	36.36
$\kappa_{s,3}$, deg	27.2	26.9	26.16	34.46	31.76	27.56
$\kappa_{p,3}$, deg	35.7	36.0	36.74	44.46	41.76	40.56
t, in.	0.0896	0.1186	0.1636	0.0951	0.1541	0.2055
σ	1.093	1.143	1.210	1.486	1.352	1.245
c, in.	1.504	1.725	1.972	1.798	1.796	1.787
l/c	0.0964	0.1858	0.2481	0	0.2773	0.3530
r_{ℓ}/s	3.215	2.550	1.9709	4.093	2.208	1.422
N	25			25		
ϵ, deg	0			45		
r_t, in.	6.720			6.720		
r_n, in.	5.188			5.188		
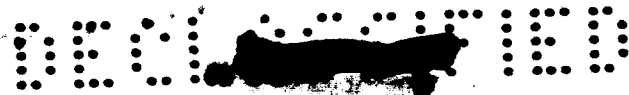
E-236

CF-3 back

TABLE II. - STATOR BLADE COORDINATES

(a) Straight blade
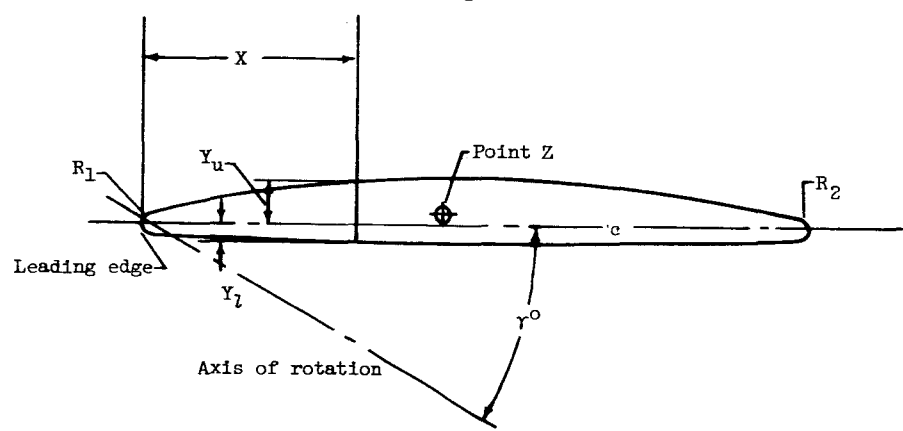
Typical airfoil section, no scale. Points Z form a line parallel to a radial line and perpendicular to airfoil sections.

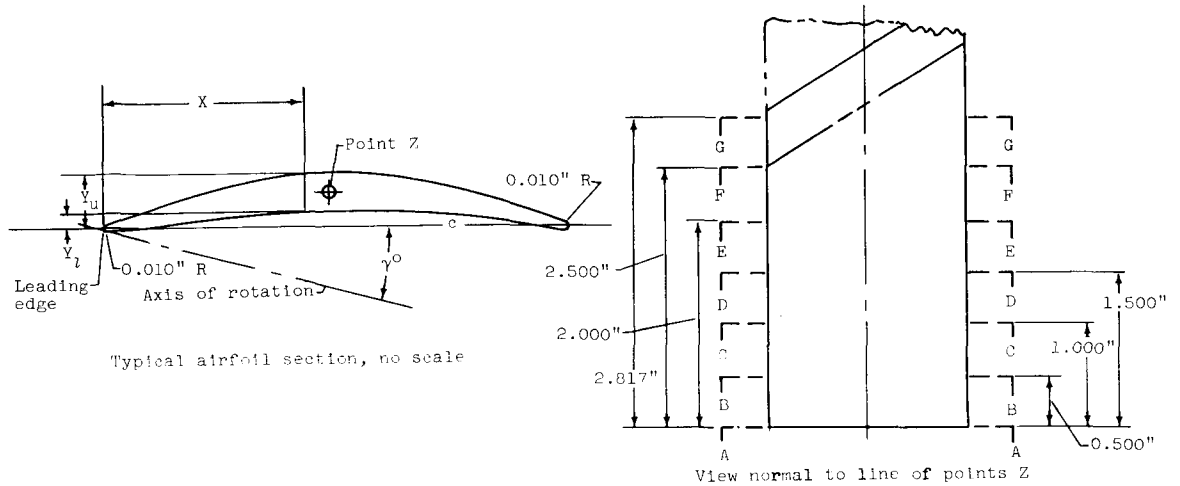| X, in.	Blade coordinates, full size, in.							
	r = 4.875 in.		r = 5.470 in.		r = 6.000 in.		r = 6.483 in.	
	Y_l	Y_u	Y_l	Y_u	Y_l	Y_u	Y_l	Y_u
0	0	0	0	0	0	0	0	0
.1	-.012	.025	-.011	.025	-.010	.032	-.011	.039
.2	-.013	.038	-.011	.039	-.010	.050	-.011	.063
.3	-.013	.048	-.012	.051	-.011	.064	-.012	.084
.4	-.013	.056	-.013	.060	-.011	.077	-.013	.101
.5	-.014	.061	-.014	.066	-.011	.087	-.013	.118
.6	-.014	.064	-.014	.070	-.012	.094	-.014	.129
.7	-.014	.064	-.014	.072	-.012	.099	-.015	.137
.8	-.013	.062	-.014	.072	-.013	.101	-.015	.142
.9	-.013	.057	-.014	.070	-.014	.101	-.015	.145
1.0	-.012	.050	-.013	.066	-.013	.098	-.016	.144
1.1	-.012	.040	-.012	.059	-.013	.092	-.016	.140
1.2	-.011	.027	-.012	.050	-.012	.084	-.016	.133
1.3	-.010	.014	-.011	.038	-.012	.074	-.015	.123
1.337	0	0	-----	-----	-----	-----	-----	-----
1.4			-.011	.025	-.011	.060	-.014	.110
1.5			0	0	-.011	.044	-.013	.092
1.6					-.010	.030	-.013	.075
1.7					-.010	.014	-.012	.057
1.723					0	0	-----	-----
1.8							-.011	.038
1.9							-.011	.021
1.971							0	0
Coordinates of point Z								
X, in.	1.011		1.011		1.011		1.011	
Y, in.	0.045		0.041		0.036		0.022	
$r°$	34°58'		35°16'		35°39'		36°15'	
R_1, in.	0.012		0.011		0.010		0.011	
R_2, in.	0.010		0.011		0.010		0.011	

E-236

TABLE II. - Concluded. STATOR BLADE COORDINATES

(b) Tilted blade

Typical airfoil section, no scale

View normal to line of points Z

|	Blade coordinates, full size, in.													
	A-A		B-B		C-C		D-D		E-E		F-F		G-G	
γ°	14°51'		20°15'		21°21'		20°48'		19°57'		19°17'		19°39'	
X, in.	Y_l	Y_u	Y_l	Y_u	Y_l	Y_u	Y_l	Y_u	Y_l	Y_u	Y_l	Y_u	Y_l	Y_u
0	0	0	0	0	0	0	0	0	0	0	0	0	0	0
.118	-.006	.039	-.007	.033	-.009	.037	-.013	.042	-.013	.051	-.017	.059	-.019	.067
.236	.001	.067	-.001	.052	-.003	.057	-.013	.068	-.015	.055	-.021	.103	-.024	.116
.354	.005	.090	.004	.070	-.005	.073	-.013	.088	-.018	.110	-.022	.134	-.026	.151
.472	.004	.111	.008	.084	-.002	.086	-.013	.103	-.018	.127	-.024	.158	-.027	.176
.590			.012	.094	0	.098	-.013	.111	-.018	.136	-.022	.173	-.027	.193
.708			.013	.100	.001	.103	-.013	.116	-.018	.138	-.022	.180	-.027	.200
.825			.014	.103	.002	.104	-.012	.114	-.017	.136	-.022	.180	-.026	.202
.943	Any curve or straight line	Any curve	.015	.103	.002	.101	-.012	.111	-.017	.129	-.021	.171	-.025	.197
1.061			.014	.100	.002	.097	-.012	.104	-.015	.114	-.021	.153	-.024	.184
1.179			.012	.094	.002	.091	-.011	.092	-.015	.096	-.020	.130	-.021	.165
1.297			.011	.086	.001	.080	-.011	.078	-.014	.078	-.019	.100	-.019	.136
1.415			.006	.073	0	.067	-.011	.062	-.013	.060	-.015	.074	-.016	.105
1.533			0	.058	-.002	.050	-.012	.045	-.012	.055	-.012	.052	-.015	.073
1.651			-.005	.039	-.006	.033	-.014	.027	-.012	.027	-.012	.029	-.013	.044
1.764			-----	-----	-----	-----	-----	-----	-----	-----	-----	-----	-----	-----
1.765			-----	-----	-----	-----	-----	-----	-----	-----	0	0	-----	-----
1.768			-----	-----	-----	-----	-----	-----	0	0	-----	-----	-----	-----
1.769			-.011	.015	-.009	.008	-----	-----	-----	-----	-----	-----	-.012	.017
1.791			-----	-----	-----	-----	0	0	-----	-----	-----	-----	-----	-----
1.795			-----	-----	0	0	-----	-----	-----	-----	-----	-----	-----	-----
1.796			0	0	-----	-----	-----	-----	-----	-----	-----	-----	0	0
1.798	0	0	-----	-----	-----	-----	-----	-----	-----	-----	-----	-----	-----	-----
Coordinates of point Z														
X, in.	0.921		0.916		0.908		0.908		0.907		0.918		0.929	
Y, in.	0.230		0.090		0.038		0.031		0.046		0.068		0.085	

E-236
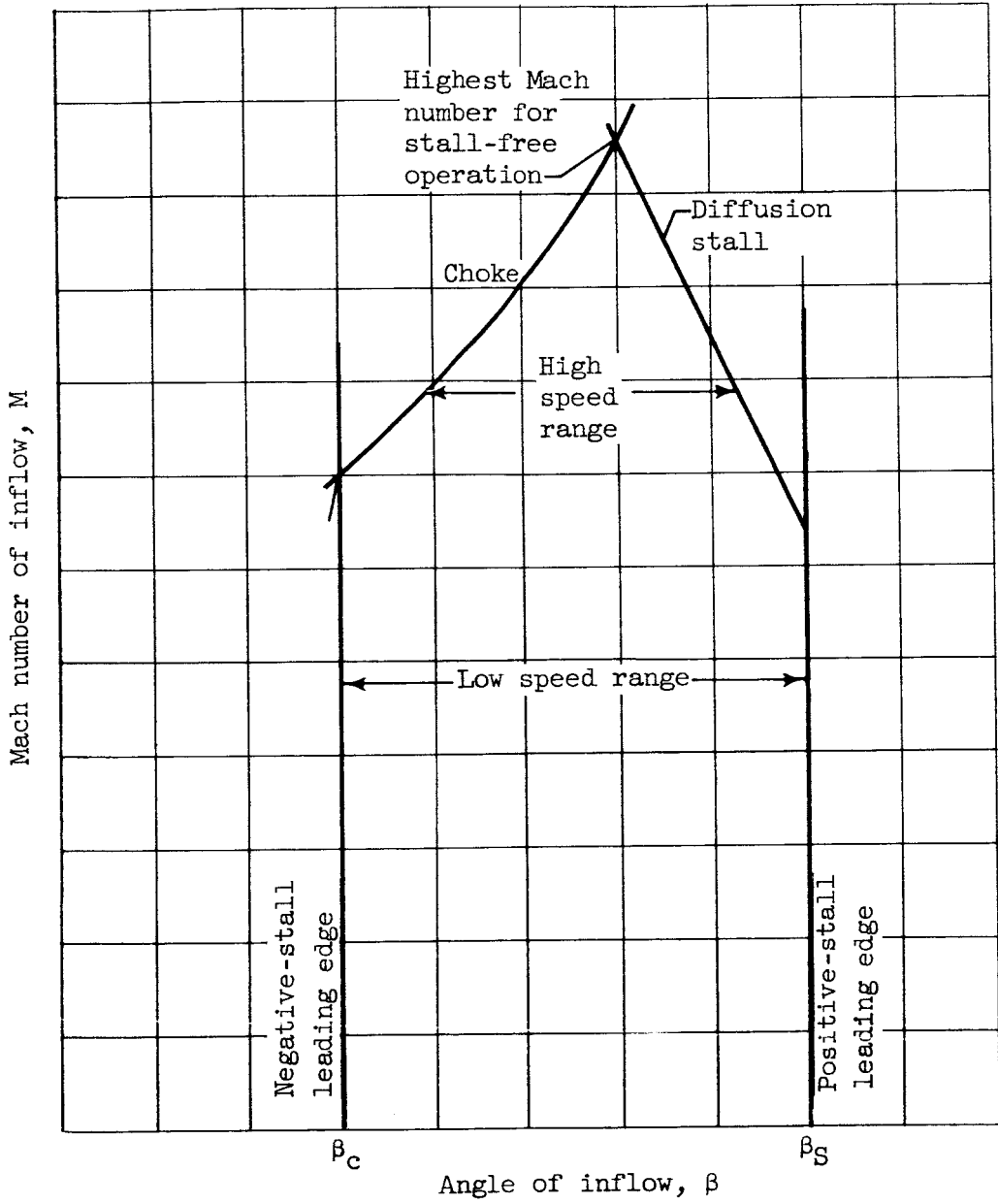
Figure 1. - Limits on operating range of a blade row.
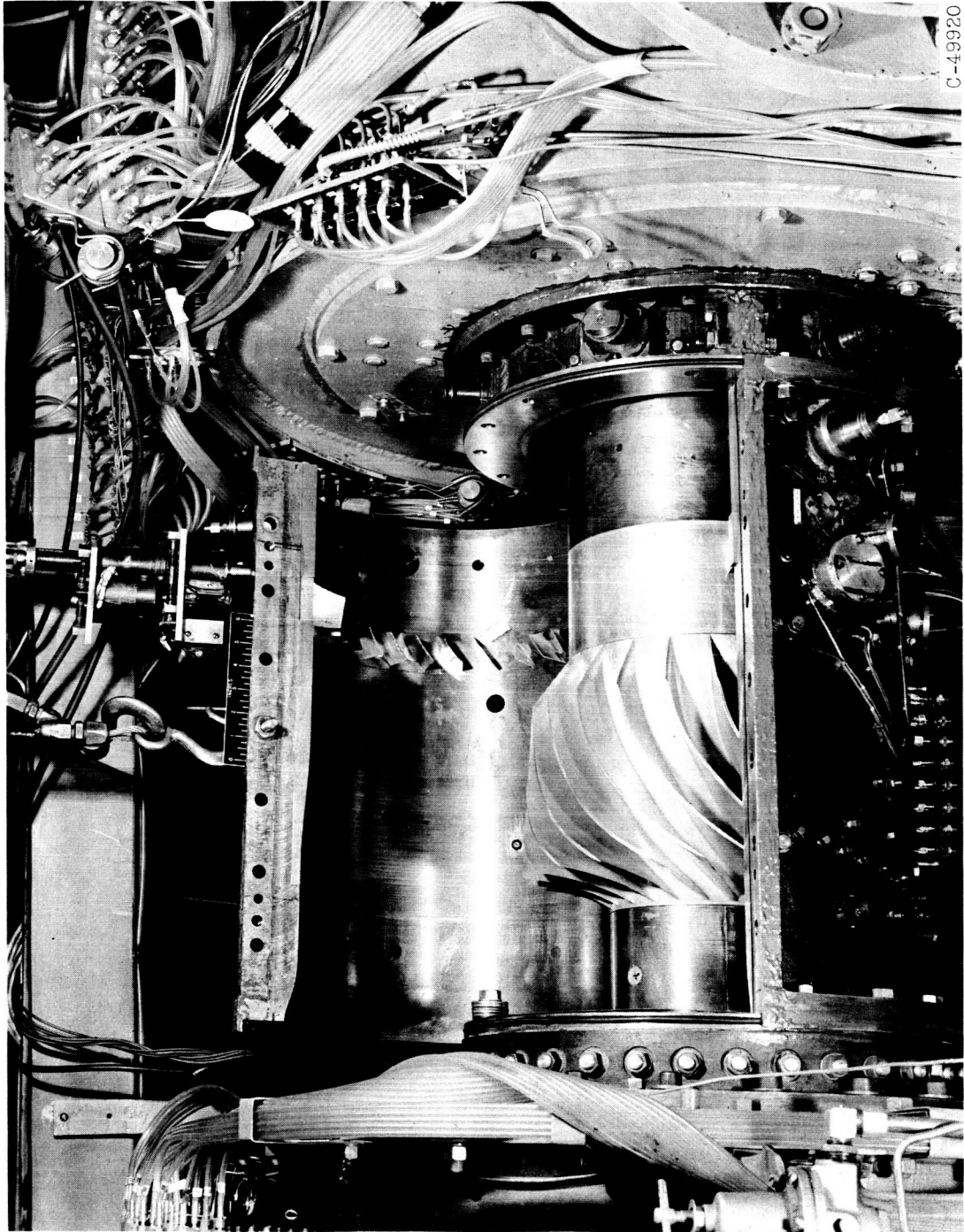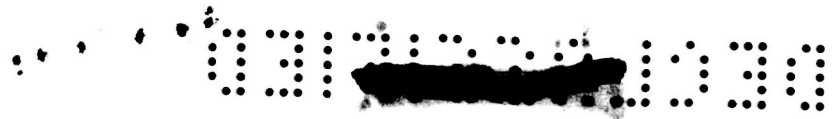
C-49920

E-236

Figure 2. - 14-Inch rotor with straight stator blades.

E-236

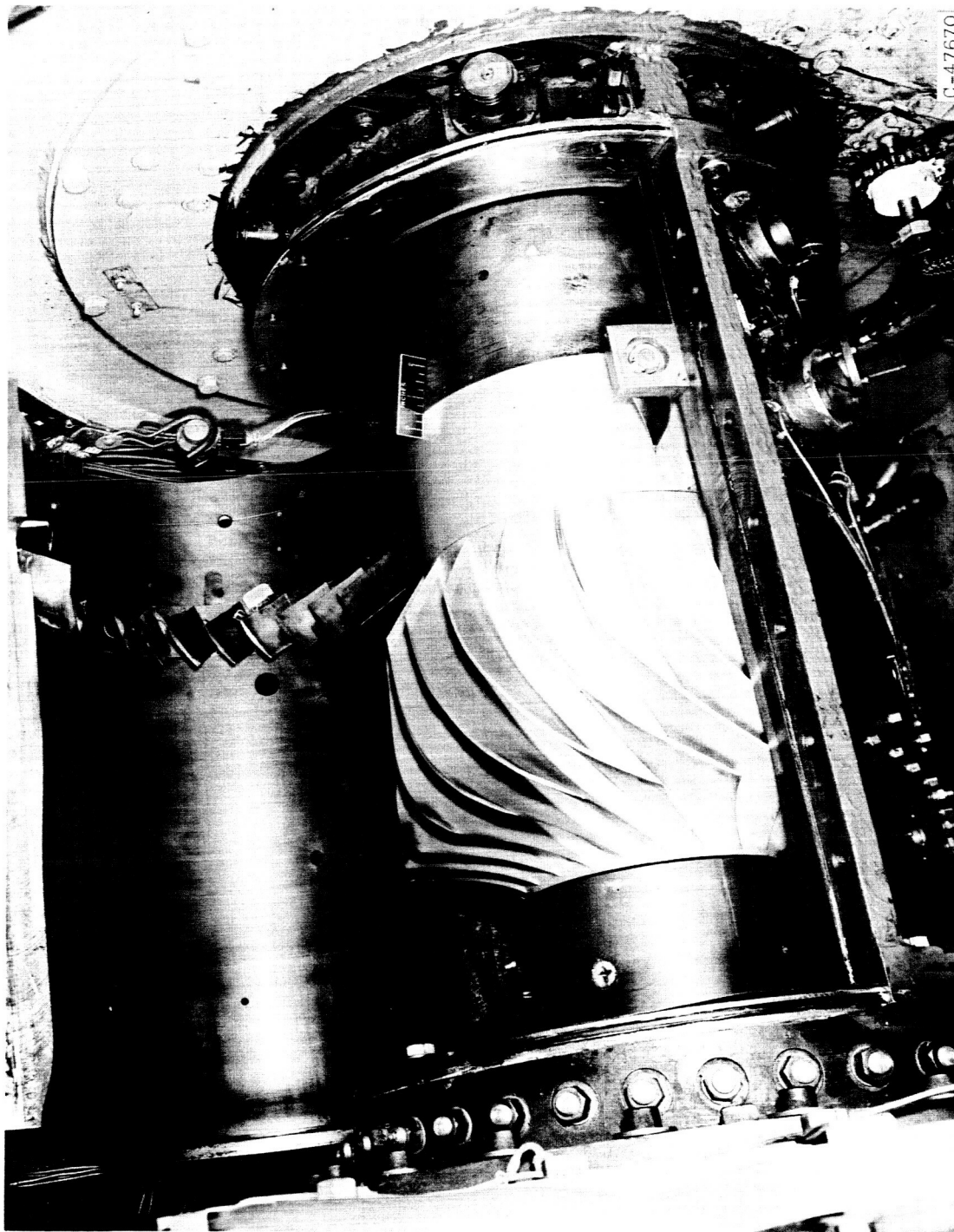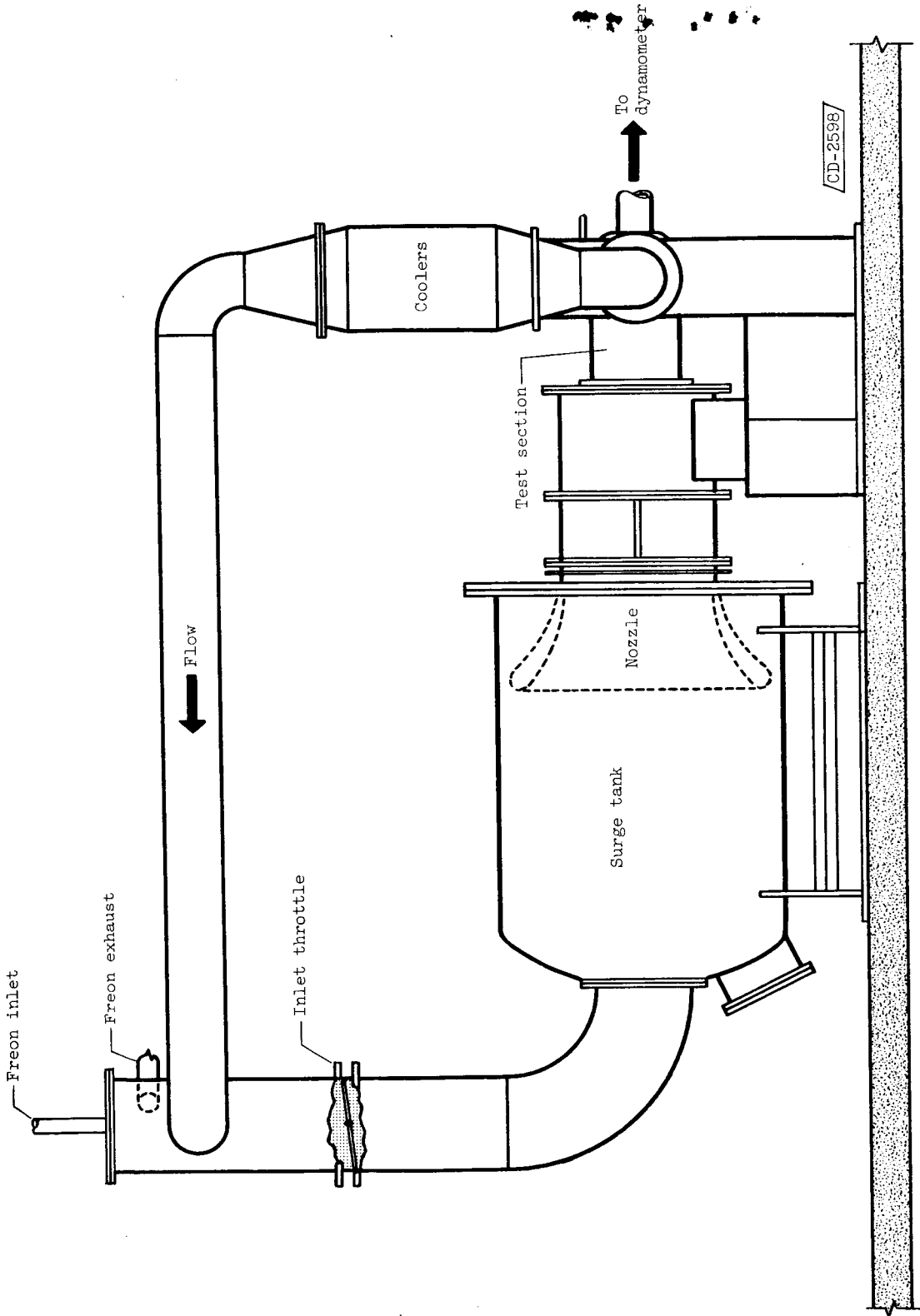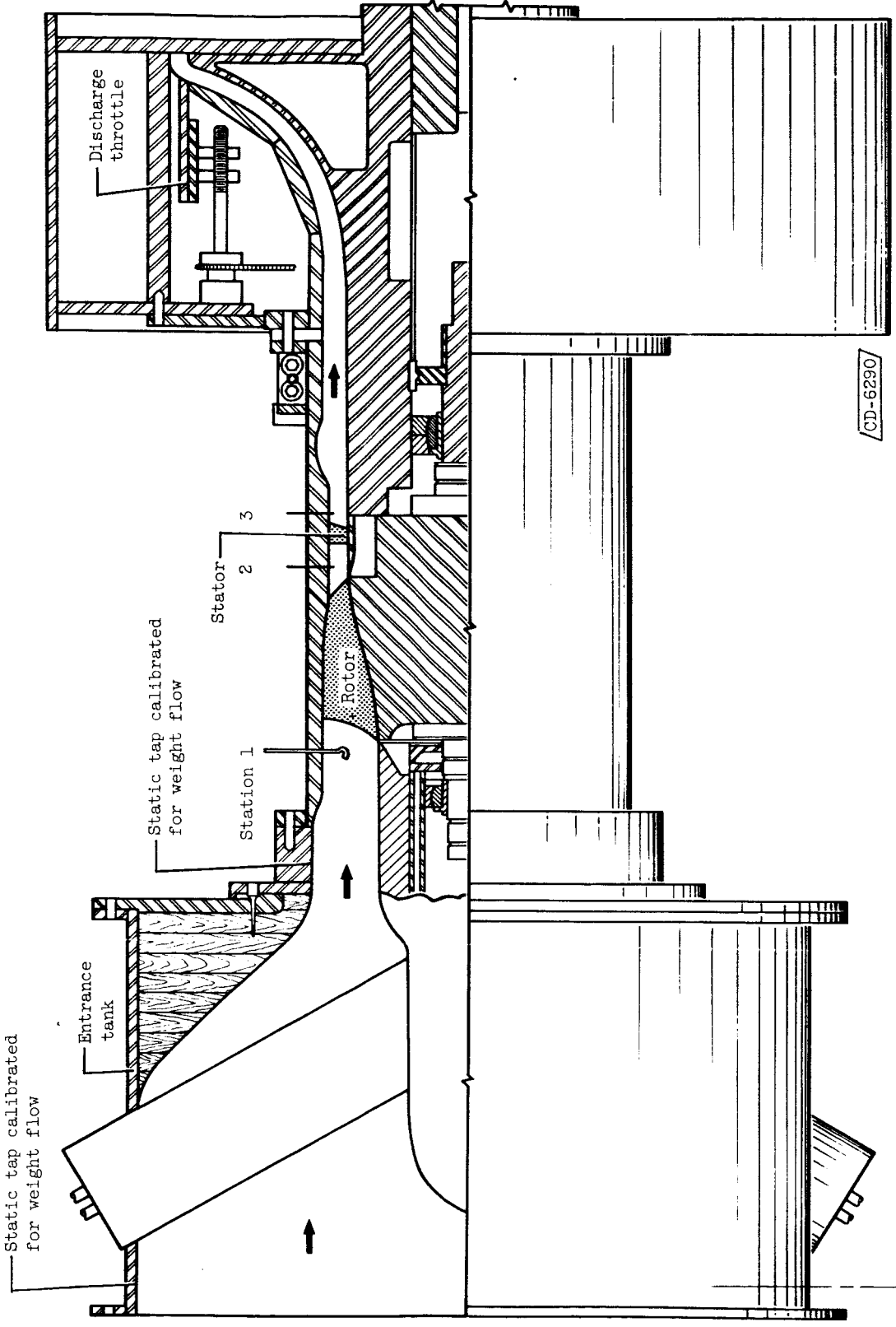Figure 3. - 14-Inch rotor with tilted stator blades.

DECLASSIFIED

To dynamometer

CD-2598

Coolers

Test section

Nozzle

Surge tank

Flow

Freon exhaust

Freon inlet

Inlet throttle

E-236

Figure 4. - Schematic diagram of piping assembly and compressor installation.

E-236

CF-4

Discharge throttle

Static tap calibrated for weight flow

Stator

2 3

Station 1

Rotor

Entrance tank

Static tap calibrated for weight flow

Station 0

CD-6290

Figure 5. - Schematic diagram of 14-inch-compressor test rig.
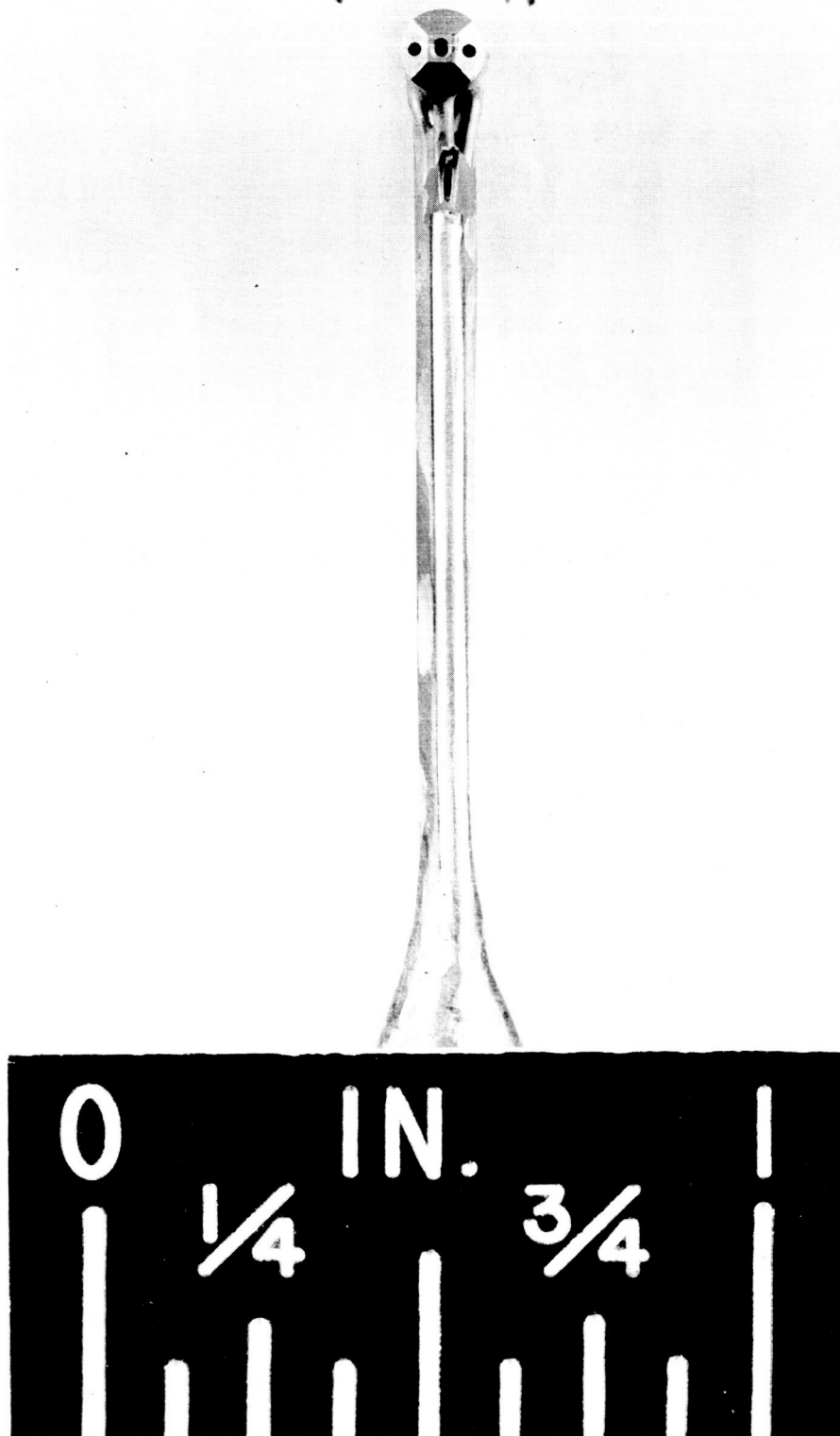
C-48342

Figure 6. - Combination probe used for measuring total pressure, total
temperature, static pressure, and flow angle.

E-236

CF-4 back
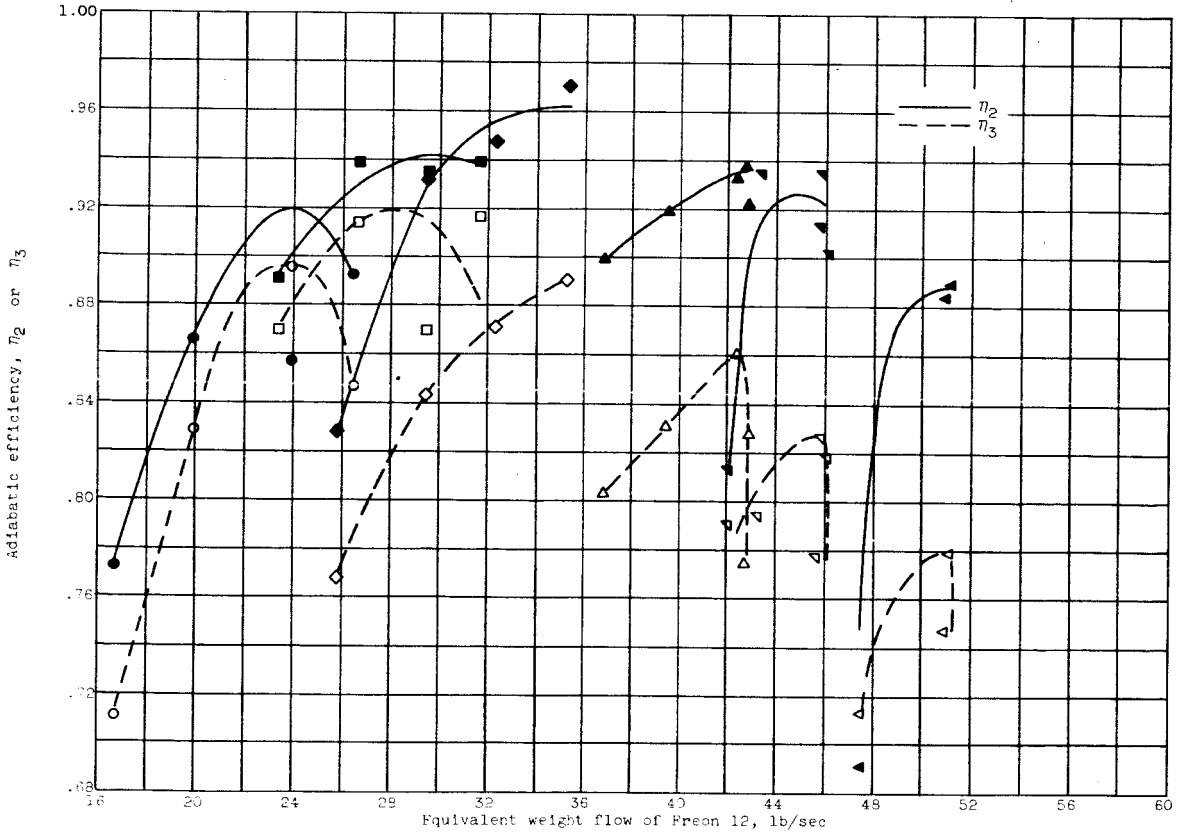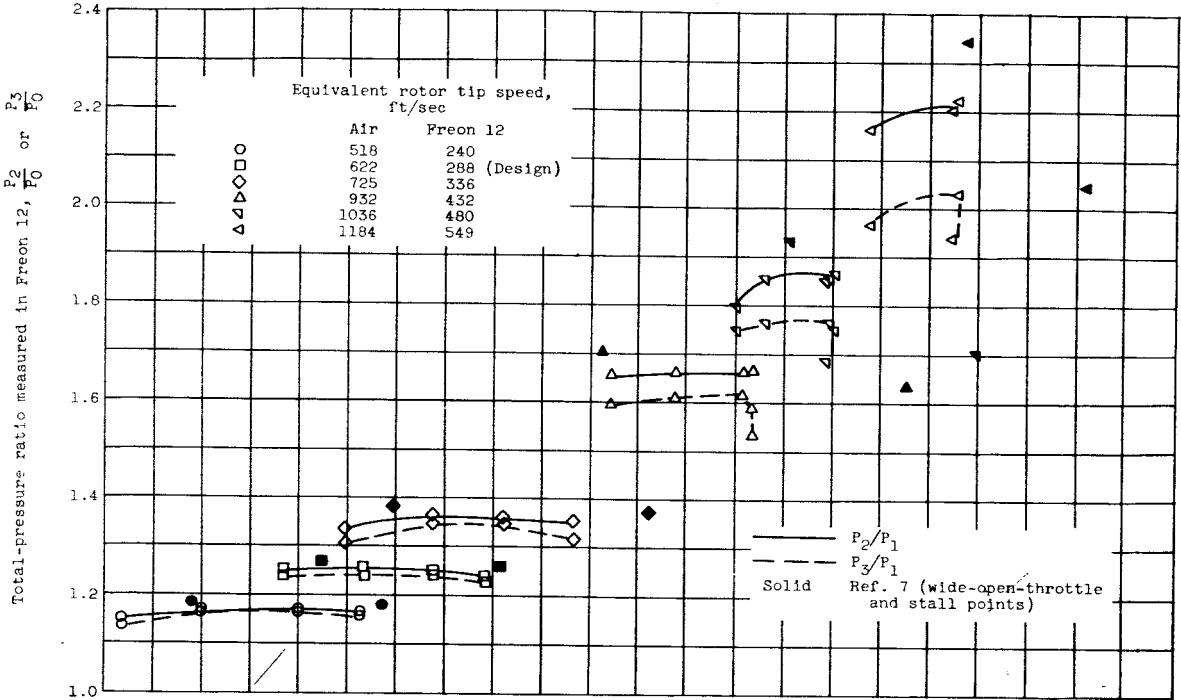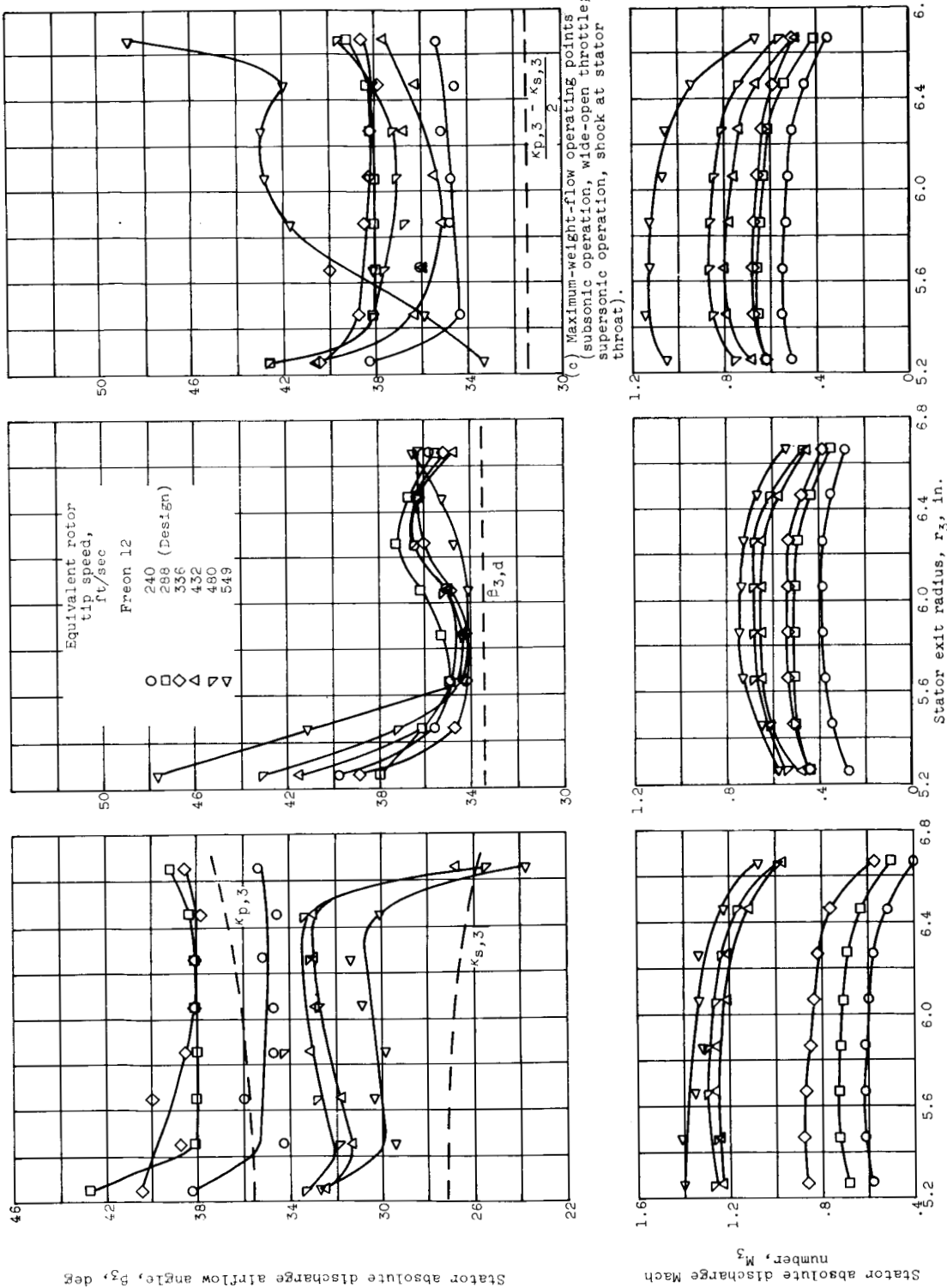

Figure 7. - Performance characteristics for straight-stator stage.
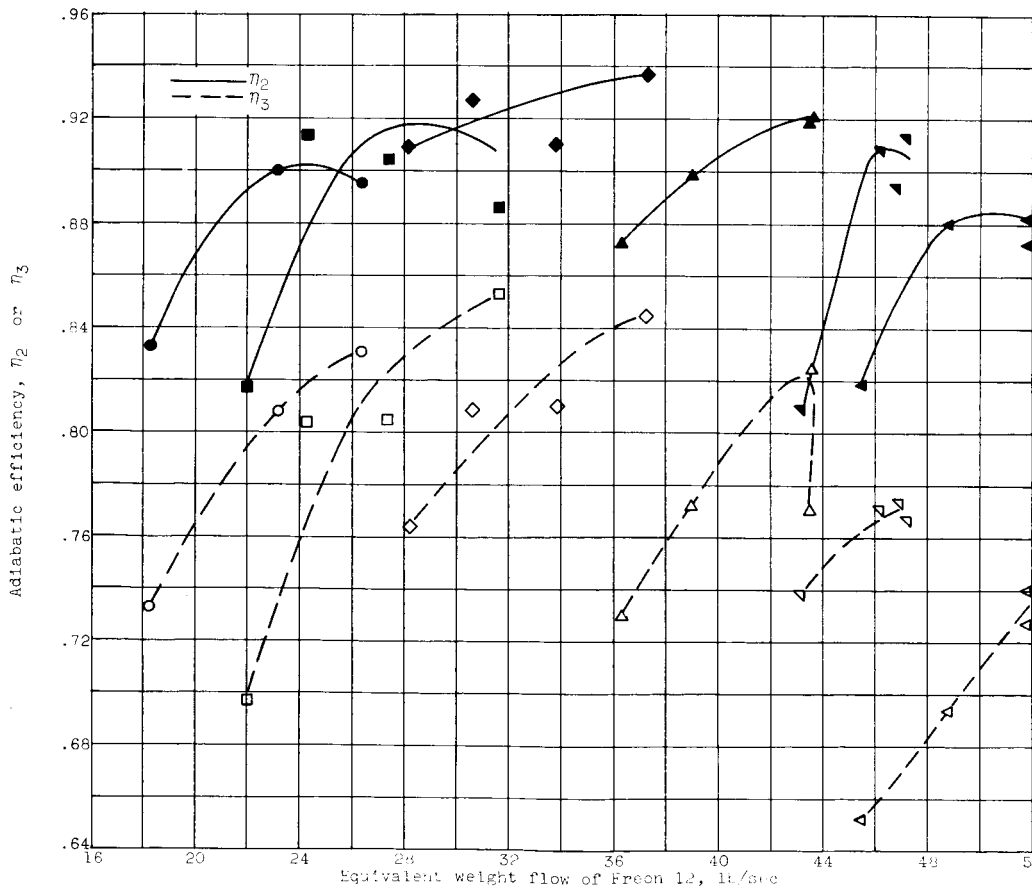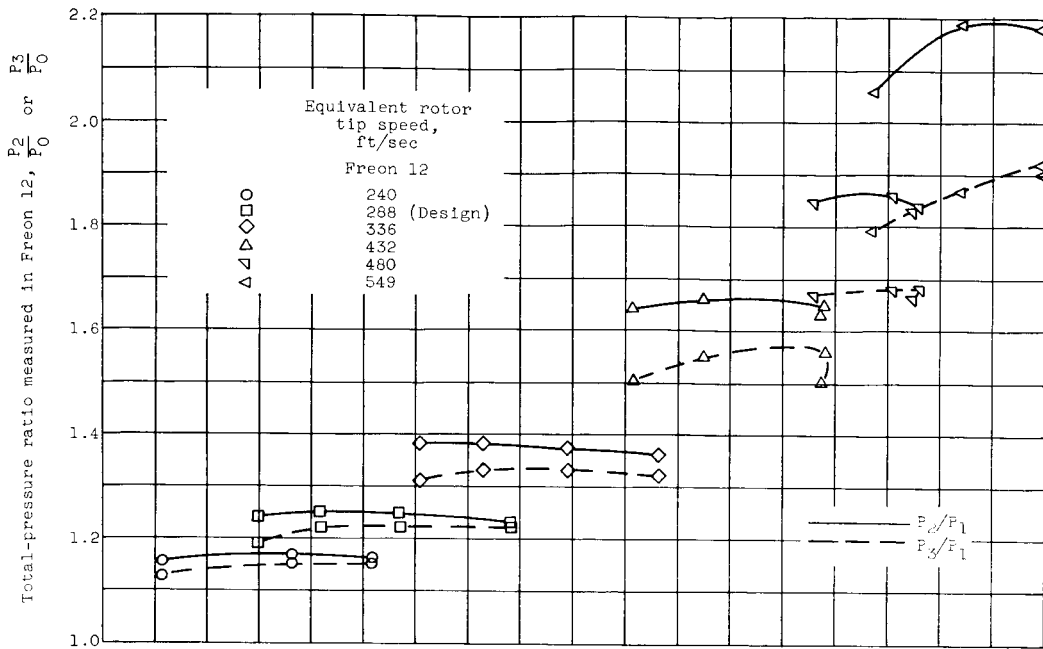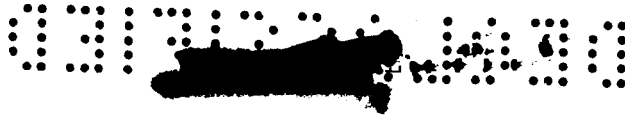
Figure 8. - Performance characteristics for tilted-stator stage.
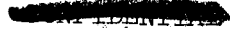
E-236
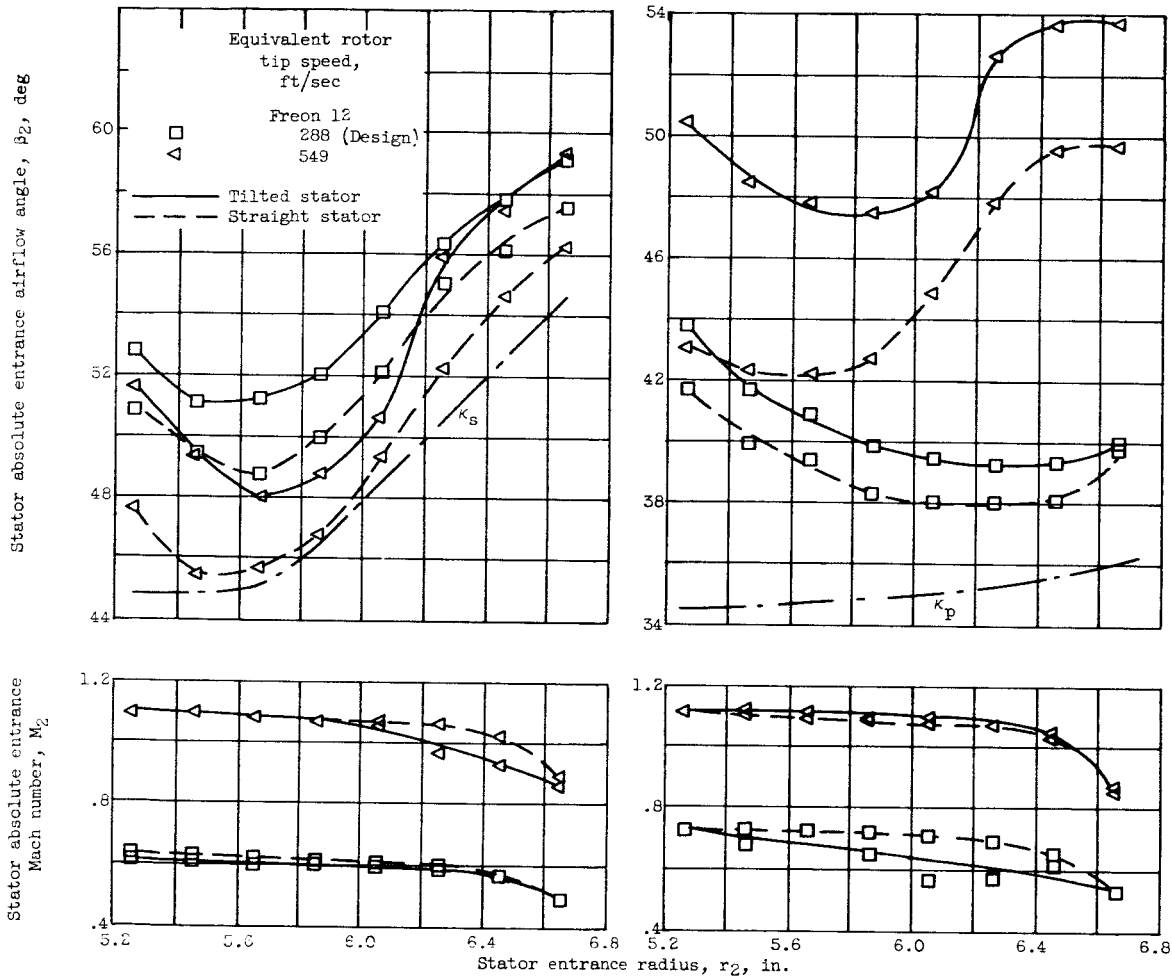
(a) Stall points.

(b) Maximum-weight-flow operating points.

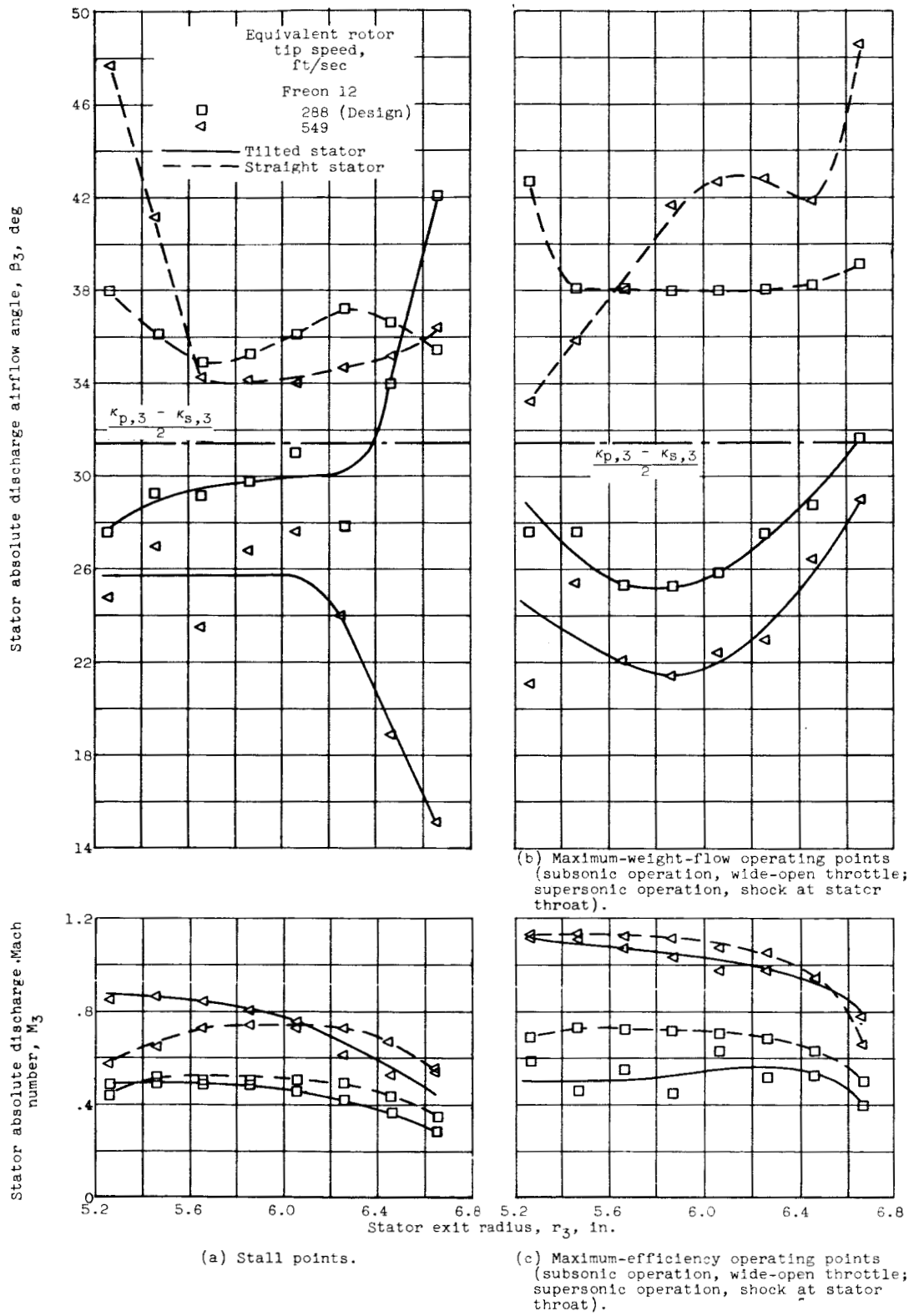Figure 9. - Conditions at stator entrance for various speeds.

E-256

Figure 10. – Straight-stator discharge flow angles and Mach numbers for various conditions.

(a) Wide-open-throttle operating points.

(b) Stall points.

(c) Maximum-weight-flow operating points (subsonic operation, wide-open throttle; supersonic operation, shock at stator throat).

(d) Maximum-efficiency operating points.

Equivalent rotor tip speed, ft/sec, Freon 12

240
288 (Design)
336
432
480
549

$\frac{K_{p,3} - K_{s,3}}{2}$

Stator exit radius, r_3, in.

Stator absolute discharge airflow angle, β_3, deg

Stator absolute discharge Mach number, M_3

(a) Stall points.

(b) Maximum-weight-flow operating points (subsonic operation, wide-open throttle; supersonic operation, shock at stator throat).

(c) Maximum-efficiency operating points (subsonic operation, wide-open throttle; supersonic operation, shock at stator throat).

Figure 11. - Stator discharge flow angles and Mach numbers for various conditions.

(a) Radius r, 5.46 inches.   (b) Radius r, 6.06 inches.   (c) Radius r, 6.46 inches.
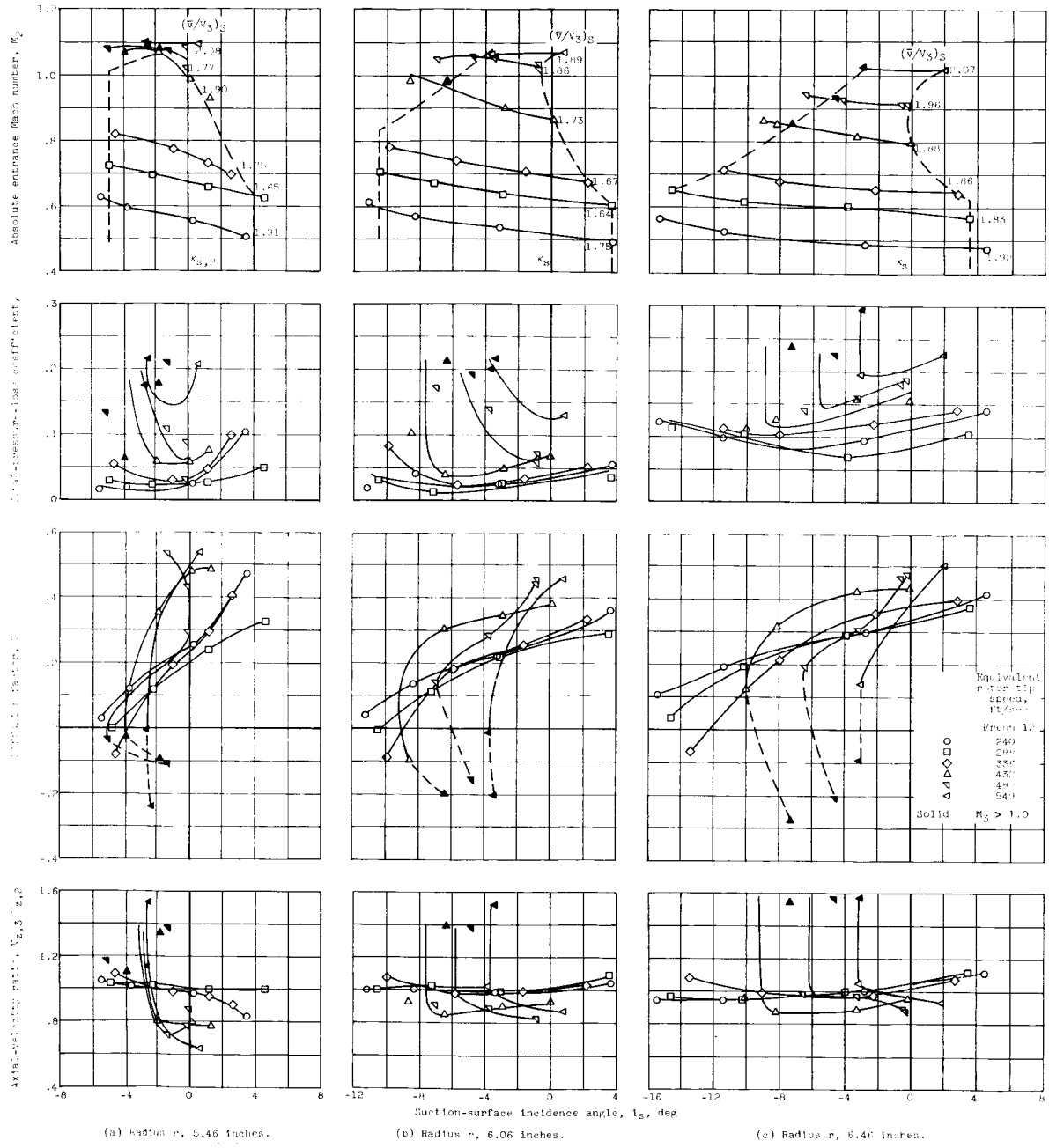
Figure 12. - Blade-element characteristics for straight stator.
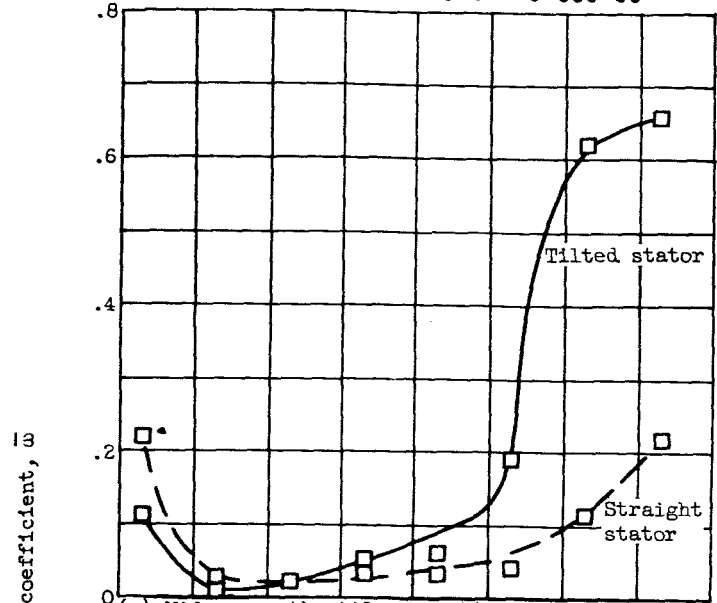
(a) Wide-open-throttle operating point. Equivalent rotor tip speed, 288 feet per second (design) in Freon 12.
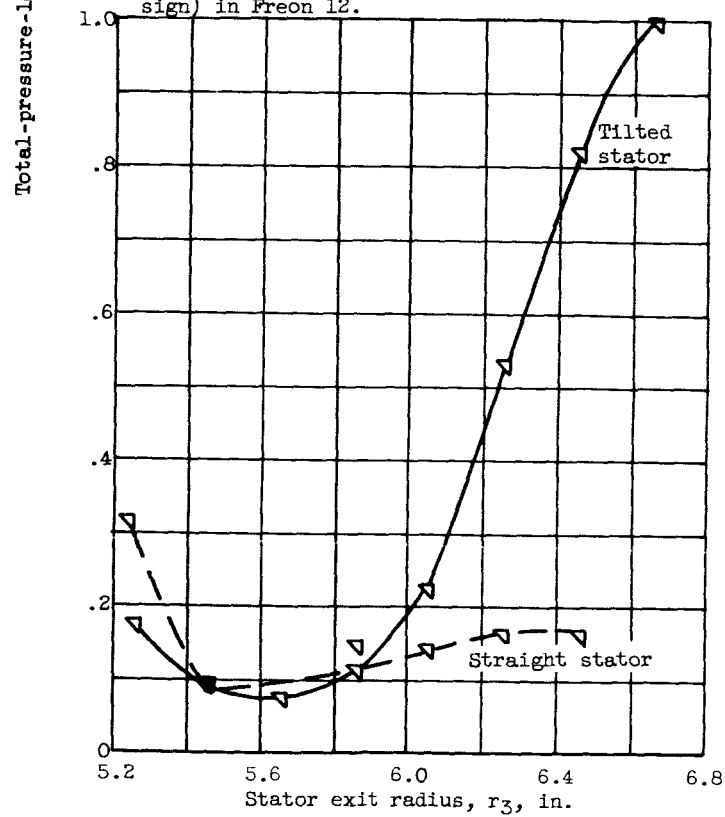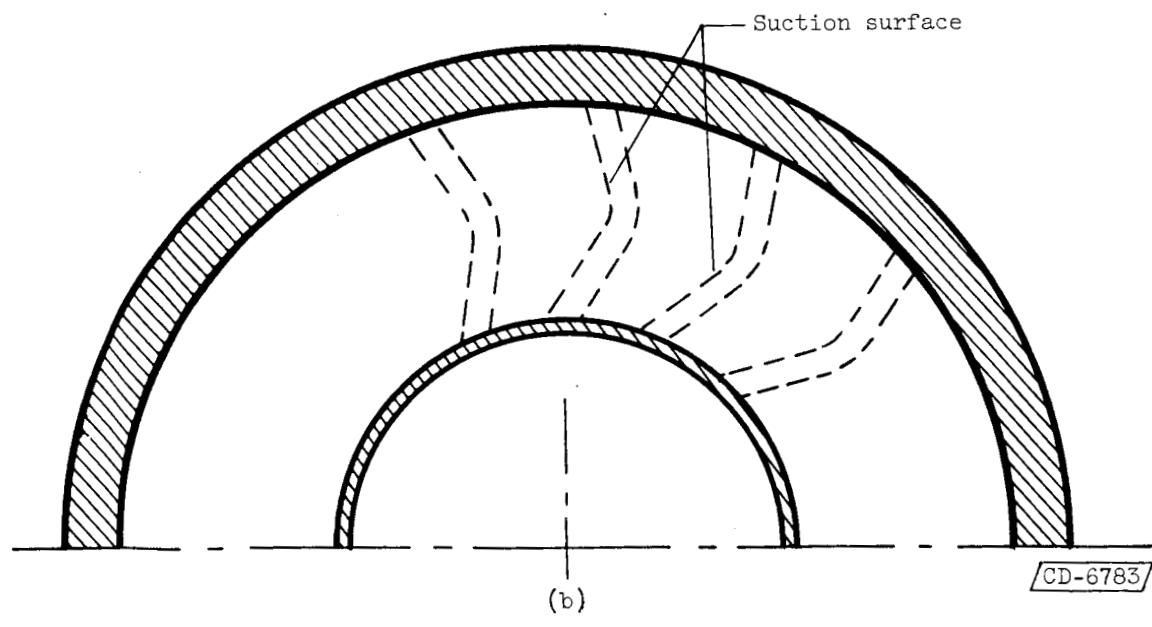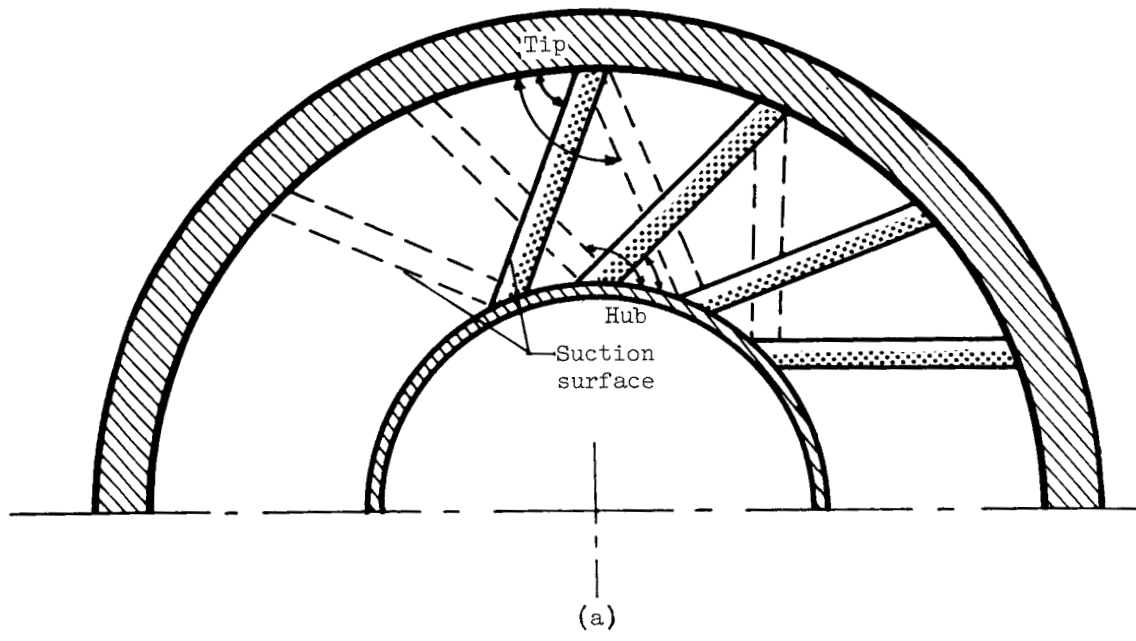
(b) Maximum-weight-flow operating point; shock at stator throat. Equivalent rotor tip speed, 480 feet per second in Freon 12.

Figure 13. - Comparison of straight- and tilted-stator blade-element characteristics.
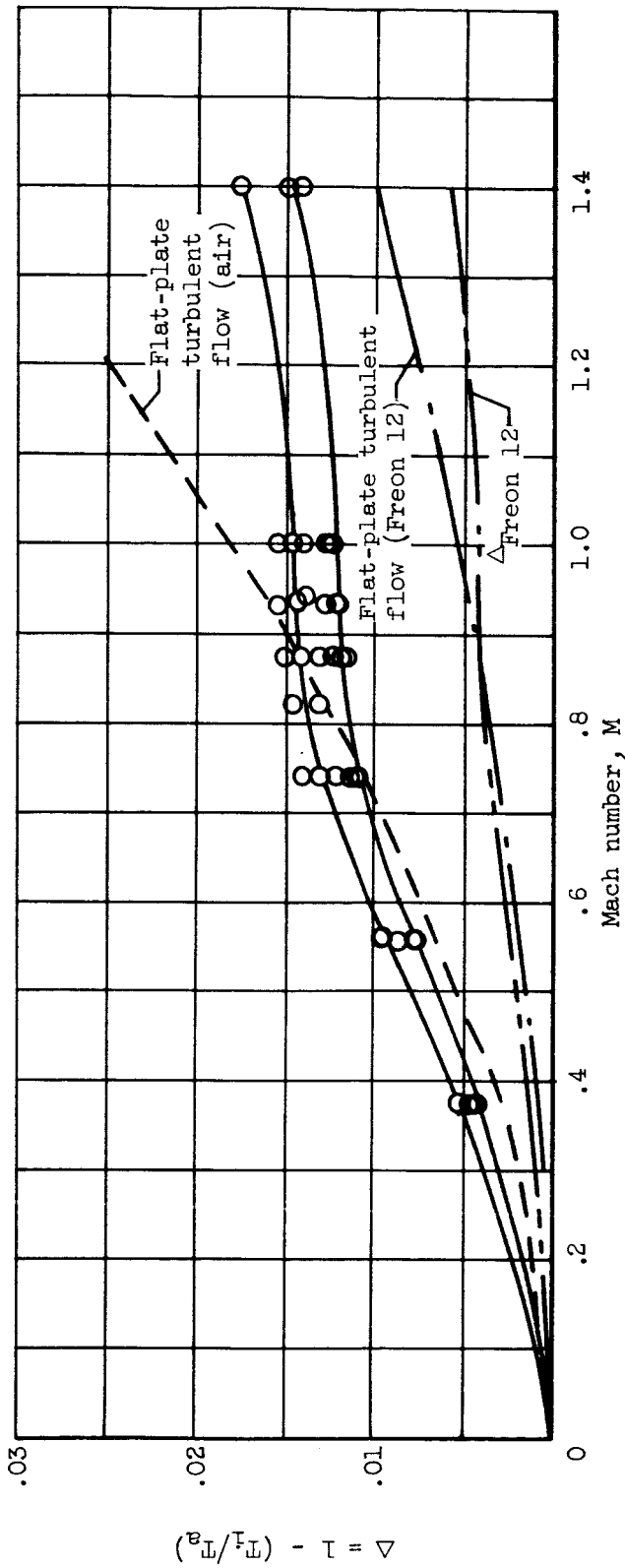
Figure 14. - Schematic diagram showing tilt.

E-236

Figure 15. - Recovery correction for six combination probes as measured in air.

$$\Delta = 1 - (T_i/T_a)$$

Flat-plate turbulent flow (air)

Flat-plate turbulent flow (Freon 12)

Freon 12

Mach number, M